NEW CONSTRAINTS ON TEMPORAL VARIATIONS IN HAWAIIAN PLUME BUOYANCY FLUX

A THESIS SUBMITTED TO THE GRADUATE DIVISION OF THE UNIVERSITY OF HAWAIʻI AT MĀNOA IN PARTIAL FULFILLMENT OF THE REQUIREMENTS FOR THE DEGREE OF

MASTER OF SCIENCE

IN

GEOLOGY & GEOPHYSICS

May 2015

By

HARRISON F.R. TOGIA

Thesis Committee:

Clinton P. Conrad, Chairperson

Garrett Apuzen-Ito

Paul Wessel

Keywords: Hawaiian swell, Hawaiian plume, mantle plume, isostatic response

Acknowledgments

This research was supported by National Science Foundation Grant EAR-1151241 and the Department of Geology and Geophysics at the University of Hawai'i at Mānoa. This paper has been greatly improved thanks to the comments and support by co-author Professor Clinton P. Conrad, committee reviewers Professor Paul Wessel and Professor Garrett Ito, and collaborator Jonathan Tree. We are grateful to Jon Sleeper for assistance with the use of GMT and Sam Howell with the use of Matlab. We also appreciate the support and encouragement from the entire Geology and Geophysics department at the University of Hawai'i at Mānoa, especially graduate students Alyssa Anderson, Brian Boston, Dana Brodie, Sara Coffey, Sarah Crites, Patrick Gasda, Kendra Lynn, Katharine Robinson, and Emma Shie.

Abstract

The Hawaiian Ridge provides a 50 million year record of the interaction between a plume of hot rock rising through the mantle and the westward motion of the Pacific plate. One feature related to the plume-lithosphere interaction, known as the 'swell', is a broad region of elevated bathymetry dynamically supported by the thermal buoyancy of plume material accumulating beneath the lithosphere. Prior studies have examined changes in swell dimensions to estimate fluctuations in the rate at which hot mantle material flows through the Hawaiian plume (buoyancy flux) to the base of the lithosphere. To improve upon these estimates, we developed a method to constrain fluctuations in Hawaiian plume buoyancy flux from swell size, using a model of the deforming plume head that assumes non-Newtonian rheology, while accounting for changes in the velocity of the Pacific plate and subsidence of the swell attributed to heat loss. To analyze the isolated signal of the swell we sampled cross sections of the swell from modern bathymetric datasets, corrected for ocean sediment thicknesses and lithospheric subsidence. By comparing these observations with model predictions of swell shape, we constrain the plume buoyancy flux over time. Our results show that the buoyancy flux of the Hawaiian plume has more than doubled between ~50 Ma and the present, and suggest that these apparent changes in flux are not associated with plume motion. Our method shows promise for understanding the time-history of plume dynamics at other hotspot ridges. Such constraints should improve our understanding of the dynamics of mantle plumes as well as the heat flow and geochemical structure of the mantle.

Table of Contents

List of Figures

1. Introduction

The Hawaiian mantle plume has sustained the growth and evolution of the Hawaiian-Emperor Ridge for more than 80 million years. Originally envisioned as a heat source fixed in the mantle, the Hawaiian plume is thought to be a conduit of thermally buoyant mantle material rising to the base of the lithosphere from a source near the core-mantle boundary [Wilson, 1963; Morgan, 1971]. As material from the plume pools beneath the lithosphere, it spreads laterally and is drawn northwest along with plate motion. Density heterogeneity between the hot deforming plume head and the cooler surrounding asthenosphere causes dynamic uplift of the local plate, resulting in a region of shallow bathymetry roughly 3000 km long and 1000 km wide known as the 'Hawaiian Swell' [Li et al., 2004] (Fig. 1). As the dimensions and scale of the swell are indicative of the rate at which plume material is ponded beneath the lithosphere [Christensen & Ribe, 1994], the presence of an elongated swell provides evidence for a long-lived upwelling plume beneath Hawaii [Sleep, 1990]. Several authors have used changes in swell dimensions along the swell axis to constrain the temporal history of plume dynamics [e.g. Sleep, 1990; Davies, 1992; Vidal & Bonneville, 2004; Asaadi et al., 2011]. Here we build upon these previous studies by incorporating new understandings of the processes by which the plume material deforms as a non-Newtonian fluid beneath the Pacific plate. In doing so, we develop new constraints on the history of buoyant material flow from the Hawaiian plume.

Davies [1988] was the first to estimate the recent buoyancy flux of the Hawaiian plume by assuming that the flux was related to the volume of swell topography. Using swell heights published by Crough [1983] and assuming a constant swell width of 1000 km, Davies [1988] suggested a present-day buoyancy flux of 6300 $kg\ s^{-1}$ for the Hawaiian plume, but acknowledged that both the delineation of swell bathymetry and a lack of insight into the complexities of plume and swell dynamics could affect this estimate. Sleep [1990] addressed the bathymetric concerns of Davies [1988] by removing the influences of lithospheric thermal subsidence and oceanic sedimentation

from swell bathymetry. Sleep [1990] further improved upon the estimates of Davies [1988] by incorporating new estimates of Pacific plate velocity near Hawaii, which is an integral part of the plume-swell relationship. Sleep [1990] concluded that 8700 $kg\ s^{-1}$ was a better estimate of recent Hawaiian plume buoyancy flux.

To constrain the time history of Hawaiian buoyancy flux, Davies [1992] determined a scaling equation relating buoyancy flux to the cross-sectional area of swell bathymetry. By analyzing cross-sections of swell bathymetry at increasing distances (and thus increasing ages) from the active hotspot center, Davies [1992] was able to infer a history of buoyancy fluxes for the Hawaiian plume going back nearly 40 million years. Vidal and Bonneville [2004] improved on this time history by filtering out the islands, seamounts, and other high frequency features that are not associated with the longer-wavelength form of the swell, improving the constraints on swell area. Most recently, King & Adams [2014] updated buoyancy flux estimates for hotspots across the globe by applying the methodologies of Davies [1992], Sleep [1990], and Vidal and Bonneville [2004] to contemporary data sets. King & Adams [2014] concluded that while current methods may suggest recent Hawaiian buoyancy flux between 4660 and 7100 $kg\ s^{-1}$, ambiguities in the characterization of swell bathymetry and assumptions of the scaling equations suggest that significant uncertainties remain.

We develop a new approach to Hawaiian swell analysis that improves upon previous analyses in three ways. First, and most importantly, we focus on the scaling equations used to relate swell dimensions to plume flux rates. While both Vidal and Bonneville [2004] and Sleep [1990] utilized a direct relationship between plume flux and swell volume, this relationship does not take into account recent advances in our understanding of plume – lithosphere interactions. In particular, Asaadi et al. [2011] showed that the widening of the Hawaiian swell is best described by a plume deformation model that assumes non-Newtonian rheology for the ponding plume material. Accounting for the physics of swell spreading allows us to utilize information from the observable

geometry of the swell, such as swell height and width, instead of modeled cross-sectional area, to constrain past plume flux.

Unlike Asaadi et al. [2011], many models of the Hawaiian plume have assumed Newtonian rheology for the lateral spreading of plume material beneath the lithosphere [Olson, 1990; Sleep, 1990; Davies, 1992; Christensen & Ribe, 1994; Moore et al., 1998; Christensen & Ribe, 1999; Zhong & Watts, 2002; King & Adams, 2014]. Under the assumption of Newtonian rheology, associated with diffusion creep deformation, the plume head continues to spread laterally as it moves away from the hotspot center (Fig. 2) [Sleep, 1990; Ribe, 2004]. Asaadi et al. [2011] showed that the lateral deformation for a non-Newtonian plume head, a rheology appropriate for dislocation creep, is less efficient and is associated with a dramatic decrease in the rate of swell spreading after ~3 million years. This results in a relativly constant swell width that better reflects observations (Fig. 2). Thus, incorporating the dynamic effects of non-Newtonian rheology into the relationship between swell dimensions and plume flux should allow us to improve constraints on the history of the Hawaiian plume.

Our second improvement to previous estimates of buoyancy flux is to separate the influence of plate motion relative to the plume from the development of the swell. Previous estimates of the plume flux have assumed constant Pacific plate motion over a stationary plume, despite studies that suggest changes in the motion of the Pacific plate [O'Connor et al., 2013] and of the plume itself [Steinberger & O'Connell, 1998; Steinberger & Antretter, 2006; Tarduno et al., 2003; 2009]. Both movements result in a change of the observed motion of the plate relative to the underlying plume, which is a key parameter that determines the rate at which plume material accumulates beneath the plate [Christensen & Ribe, 1994], forming the swell. By adjusting the equations of Asaadi et al. [2011] to incorporate changes in plate motion, we account for both shifts in Pacific plate motion and motion of the plume conduit. Specficially, we incorporate two recently published progressions

for the ages of Hawaiian volcanism across the Pacific plate constrainted by O'Connor et al. [2013] (Fig. 3A). These shifts in apparent Pacific plate velocity over the Hawaiian plume affect the plume width for a given plume buoyancy flux (Fig. 2) and thus significantly change our interpretation of the plume's historical buoyancy flux.

The third and final improvement is our reevaluation of the assumption that the cooling of plume material beneath the lithosphere does not affect the interpretation of swell dimensions. Sleep [1990] and Davies [1992] both constructed simple thermal models of heat diffusion from the spreading plume material and concluded that thermal subsidence exerts a negligible influence on swell bathymetry along the Hawaiian Ridge. However, because the effects of thermal subsidence increase with time, and because we extend our analysis back to the bend in the Hawaiian-Emperor seamount chain at roughly 50 Ma, we model the slow subsidence of swell topography associated with the cooling of plume material beneath the lithosphere and correct for this effect when interpreting swell topography.

Constraints on changes in the buoyancy flux of the Hawaiian plume provide valuable insight into time-dependent plume dynamics and heat transport in the mantle. Davies [1988] and Sleep [1990] used buoyancy flux estimates for plumes around the world to help constrain theories on global mantle heat flow and deep mantle thermal structure. Measurements of time-varying buoyancy flux have also been used to infer the health and life cycle of plume source material. Sleep [1990] and King & Adams [2014] suggested that the prolonged decrease in buoyancy flux observed at the Louisville hotspot could indicate depletion of the source. A better understanding of the time-varying buoyancy flux can help us improve our understanding of the interactions between the plume and the moving lithosphere [e.g. Christensen & Ribe, 1994; 1999]. Thus, an improved estimate of the history of Hawaiian plume buoyancy flux could improve our understanding of plume dynamics and the thermal evolution of the greater mantle.

2. Evolution of Swell Topography

In order to constrain temporal changes in the buoyancy flux of the Hawaiian plume using observable variations in swell topography, we use Asaadi et al.'s [2011] analytical model for the deformation of plume material, which assumes non-Newtonian rheology. We use this model to predict swell bathymetry as a function of swell age, plume volume flux, and excess temperature. We incorporate shifts in Pacific plate velocity and a decline in swell amplitude through diffusive cooling of the plume material.

2.1 Swell Dimensions Assuming Non-Newtonian Rheology

Asaadi et al. [2011] showed that gravitational spreading of plume material beneath a plate occurs differently for dislocation creep rheology (power-law exponent $n > 1$), which exhibits non-Newtonian behavior, than it does for diffusion creep ($n = 1$), which exhibits Newtonian behavior (Fig. 2). The non-Newtonian rheology limits down-swell widths and explains the observed lack of significant widening of the Hawaiian swell along its length [Asaadi et al., 2011]. Equation 15 of Asaadi et al. [2011] describes the downstream evolution of swell half width L as

$$L(x) = c_2 L_0 \left(\frac{x-x_0}{L_0}\right)^{\frac{1}{3n+2}} \quad (1)$$

where $c_2 \approx 0.9432$ is a constants necessary for Eq. (1) to fit Asaadi et al.'s [2011] numerical solution based on lubrication theory, $(x - x_0)$ is the downstream distance from the hotspot center (x_0), and $n = 3.5$ is the power-law constant for dislocation creep. Profiles of equation 1 show that a majority of swell widening occurs within the first 3 - 5 million years of swell development, with swell widths stabilizing after this time frame (Fig 2).

The length scale L_0 [Asaadi et al., 2011, Eq.2] in Eq. (1) is described as

$$L_0 = \left(\frac{\sigma Q^{2n+1}}{U^{2n+2}}\right)^{\frac{1}{3n+1}} \quad (2)$$

where $\sigma = D\frac{(g\,\delta\rho)^n}{[(n+2)(n+3)]}$ is the lateral spreading rate of plume material along the base of the lithosphere, $D = \frac{(2+n)(3+n)\left(\frac{L_0}{g}\right)^n \delta\rho^{1+n} U}{[S_0(\rho_0-\rho_w)]^{1+2n}}$ [Asaadi et al., 2011, Eq. 23] is the rheological prefactor of the lubrication theory solution, $g = 9.81\ m\,s^{-2}$ is the gravitational acceleration of the Earth, $\delta\rho = \rho_0\alpha\,\Delta T$ is the density difference between the plume material and the ambient mantle, ΔT is the temperature difference between the ambient mantle and plume material (plume excess temperature), $\rho_0 = 3400\ kg\,m^{-3}$ is the density of the ambient mantle, $\alpha = 3 * 10^{-5}\,K^{-1}$ is the coefficient of thermal expansion of mantle material, $\rho_w = 1000\ kg\,m^{-3}$ is the density of sea water, and $S_0 = \frac{Q\delta\rho}{UL_0(\rho_0-\rho_w)}$ is the amplitude scale factor for isostatic topography [Asaadi et al., 2011, Eq. 3]. Equation 4 of Asaadi et al. [2011] describes the decay of swell height along the swell length axis, $y = 0$, as

$$S(x) = S_0\left(\frac{x-x_0}{L_0}\right)^{-\frac{1}{3n+2}} \quad (3)$$

Some uncertainty from the Asaadi et al. [2011] scaling equations is factored into our results, because the equations for swell width (Eq. 1) and amplitude (Eq. 3) are most accurate at distances of $x > 2L_0$ away from the hotspot center, but offer more approximate solutions for closer distances. We use equations 1-3 to fit the swell and thus relate the observations to changes in plume material flux (Q), excess temperature (ΔT) and therefore plume buoyancy flux. Because uncertainty associated with the scaling equations is directly connected to the interpretation of buoyancy flux, inaccuracy in the scaling equations is represented by the range of suggested buoyancy flux values.

2.2 Effects of Variations in Relative Plate Velocity on Swell Development

At constant rates of buoyancy flux, the amount of plume material pinned to the base of the lithosphere, and therefore the size of the swell, is controlled by the relative velocity of the overlying plate (U). Changes in this velocity, as measured by O'Connor et al. [2013] using volcanic ages along the Hawaiian Ridge, can be caused by changes in the motion of the plate or by lateral motion of the plume conduit beneath the lithosphere. An increase in relative plate velocity reduces the volume of plume material that can accumulate beneath any one section of the plate and thus decreases the overall width of the swell. Hence, a decrease in swell width with time could be caused by either a decrease in plume flux or an increase in relative plate velocity. Inversely, a decrease in the relative velocity causes greater pooling of plume material and a wider swell.

To account for changes in relative plate velocity (U), our first step is to identify the possible progressions of apparent plate velocities relative to the location of Hawaiian volcanism. O'Connor et al. [2013] proposed two alternative histories for the time-dependence of plate velocity along the Hawaiian Ridge. The first, denoted here as U_{27}, suggests a change at 27 Ma from a velocity of 59 $km\,Myr^{-1}$ to 87 $km\,Myr^{-1}$ until the present day. O'Connor et al.'s second velocity progression, denoted here as U_{17}, suggests a change at 17 Ma from a velocity of 59 $km\,Myr^{-1}$ to ~108.5 $km\,Myr^{-1}$(Fig 3).

In order to accommodate the variations in relative velocity within the scaling equations for swell dimensions, we introduce two alterations to the Asaadi et al. [2011] equations for the evolution of the swell. The first modification is to replace Asaadi et al.'s [2011] independent variable of distance ($x - x_0$), with an expression for time (Ut) in equations 1 and 3, where t is the age of the swell. Introducing a non-constant term for plate velocity into the Asaadi scaling equations changes the predicted ages for those sections of the swell beyond the shift in relative plate velocity. However, this effect has been accounted for because we have shifted the independent variable from distance

to time. Thus the role of distance to identify the progression of the swell is replaced by the 'time' allowed for the swell to develop.

Our second adjustment is to introduce an averaged term for relative plate velocity ($\langle U \rangle$) into the expressions for swell dimensions L_0 and S_0 and the rheological prefactor D to account for changes in plume spreading rates that result from changes in plate velocity. The swell lengths scales L_0 and S_0 are based on the plume and plate conditions at the time of swell formation. The rheological prefactor D regulates the lateral spreading of the deforming plume material beneath the lithosphere and also depends on plate velocity. Therefore, a change in apparent plate velocity U affects S_0, D and L_0 directly, but L_0 is additionally affected through its dependence on D. Together, the equations for swell widening (Eq. 1 & 2) predict that an instantaneous increase in plate velocity would lead to a rapid narrowing of swell dimensions (Fig. 2). However, because deformation of the sub-lithospheric plume material is ongoing, any change in lithospheric velocity affects the rate of change in swell width with distance for all the plume material that has previously been emplaced beneath the lithosphere. To reproduce the ongoing changes in plume spreading into our model, we use a weighted average relative plate velocity ($\langle U \rangle$) for swell development (Fig 3).

$$
\begin{aligned}
&0Ma \leq t \leq 27Ma: && \langle U_{27} \rangle = 87\ km\ Myr^{-1} \\
&t > 27Ma: && \langle U_{27} \rangle = \frac{\left[\left(27Myr * 87\ km\ Myr^{-1}\right) + \left((t-27Myr) * 59\ km\ Myr^{-1}\right)\right]}{t} \\
&0Ma \leq t \leq 17Ma: && \langle U_{17} \rangle = 108.5\ km\ Myr^{-1} \\
&t > 17Ma: && \langle U_{17} \rangle = \frac{\left[\left(17Myr * 108.5\ km\ Myr^{-1}\right) + \left((t-17Myr) * 59\ km\ Myr^{-1}\right)\right]}{t}
\end{aligned}
\qquad (4)
$$

For portions of the swell younger than the age of the proposed changes in relative velocity (17 or 27 Ma), U is constant and the solution reverts to Asaadi et al.'s [2011] constant velocity case (Fig. 2). However, for older segments, swell spreading occurs initially under a plate moving at a slower speed,

and later under a faster-moving plate. The above-described average of the two velocities accounts for the spreading that occurs beneath the changing-velocity plate, and we apply $\langle U \rangle$ in place of U in the equations for L_0, D and S_0 (in that order). Note that our use of an average velocity is an approximation for how lateral spreading rates respond to a change in relative plate velocity. Without direct constraints on this parameter, uncertainty is associated with the range of possible velocity progressions used to mimic this interaction.

2.3 Influence of Thermal Diffusion on Swell Magnitude

Because the buoyant uplift of the swell is derived from the thermal differential between the plume and the ambient mantle, the plume excess temperature (ΔT) directly influences swell height. As time passes, heat diffuses from the plume material through the lithosphere and the ambient asthenosphere. Depending on the thickness of the lithosphere, some of this heat will escape through the ocean floor as the plume-lithosphere system cools. This cooling decreases the buoyancy that dynamically forms the swell. Therefore, we incorporate changes in swell height associated with the cooling of plume material into our model for swell development. To account for the cooling of the system, our model uses an error function solution for the diffusive heat equation for temperature at depth (Fig. 4A), expressed as [Turcotte & Schubert, 2002]

$$T(z,t) = \left(\frac{\Delta T}{2}\right)\left[\left(\frac{\mathrm{erf}\,(z-h_l)}{2\sqrt{kt}}\right) + \left(\frac{\mathrm{erf}\,(z+h_l)}{2\sqrt{kt}}\right) - \left(\frac{\mathrm{erf}\,\left(z-(h_l+h_p)\right)}{2\sqrt{kt}}\right) - \left(\frac{\mathrm{erf}\,\left(z+(h_l+h_p)\right)}{2\sqrt{kt}}\right)\right] \qquad (5)$$

where ΔT is the excess temperature of the plume at $t = 0$ Ma, z is depth, $h_l = 75$ km is the thickness of the lithosphere appropriate for the Hawaiian Ridge, $h_p = 100$ km is the thickness of the plume material, and $\kappa = 1\ mm^2\ s^{-1}$ is the coefficient of thermal diffusivity of mantle material. The first and second error functions represent thermal diffusion across the plume-lithosphere boundary. Similarly, the third and fourth error functions represent thermal diffusion across the boundary between the plume and the surrounding mantle. Initially the temperature contrast between the

lithosphere and the plume is sharp, as heat has not had time to diffuse into the lithosphere (Fig. 4A). As time passes, heat diffuses from the plume material into the lithosphere and surrounding mantle, cooling the buoyant plume material and smoothing the temperature profile (Fig. 4A). However, after some time, heat from the plume material reaches the surface of the plate and cools the system, decreasing the total swell buoyancy (Fig. 4B). A decrease in the area beneath the temperature curve is proportional to the heat lost from the system via diffusion. So, using the relationships between the change in temperature and dynamic support, the height of the swell (Eq. 3) can be scaled as

$$H(t) = S(t)\left(\frac{\int_{500}^{0\ km} T(z,t)\,\partial z}{\int_{500}^{0\ km} T(z,0\ Ma)\partial z}\right) \quad (6)$$

where $H(t)$ is the adjusted swell height, $S(t)$ is the amplitude of the swell calculated by equation 3 (with x expressed as Ut), $T(z,t)$ is the temperature at depth (Eq. 5), and t is the age of the observed swell. This simplified model shows that diffusive cooling of underpinned plume material results in a ~4% decrease in the buoyancy of the plume material over 47.5 Ma, which is roughly the life of the swell (Fig. 4B). Despite a small change, we incorporate this diffusive cooling as a part of our swell analysis model.

3. Constraining Hawaiian Buoyancy Flux

In order to constrain variations in buoyancy flux as a function of time, we compare predicted swell dimensions with observed bathymetry along transects drawn across the swell.

3.1 Isolating Swell Bathymetry

To better constrain variations in historic buoyancy flux from swell topography, we isolate the bathymetric expression of the swell using a technique similar to that of Sleep [1990] and King & Adams [2014]. We begin by correcting the 1 minute bathymetric grid ETOPO1 [Amante & Eakins, 2009] for the affects of sediment loading and lithospheric subsidence (Fig. 1). To remove the

bathymetric effects of sediments, we apply the Sykes' [1996] correction for isostatically compensated sediments

$$\Delta z_{sed} = 0.43422d - 0.010395d^2 \quad (7)$$

where Δz_{sed} stands for isostatic compensation depth, and d is the sediment thicknesses obtained from Divins [2003]. To correct for seafloor subsidence with age, we utilize the methodology developed by Hillier & Watts [2005], which was later confirmed for the entire Pacific by Zhong et al.. [2007], that describes subsidence as

$$\Delta z_{age} = 3010 + 307t^{\frac{1}{2}} \quad \text{for } t < 85 \text{ Ma}$$

$$\Delta z_{age} = 6120 - 3010\exp(-0.026t) \quad \text{for } t > 85 \text{ Ma} \quad (8)$$

where Δz_{age} is the thermal subsidence depth in meters and t is the age of the sea floor. The corrected bathymetry is determined as

$$Z_{corr} = z_{bath} - \Delta z_{age} - \Delta z_{sed} \quad (9)$$

From the corrected bathymetry, we complete our isolation of the swell by reducing short wavelength signals using the methodology of Wessel [1998]. Because the swell is roughly 1000 km wide and 3000 km long, it features length scales that are much greater than those of the islands or seamounts that lie atop the swell, which are only hundreds of kilometers wide. To isolate the long wavelength features of the swell, we implement the same 465 km radial median filter chosen specifically for Hawaii by Wessel [1998] (Fig. 5). To compare the predicted swell dimensions to the bathymetry, we sample the filtered topography along the ridge between 155.8658W/20.2854N and 173.9674E/32.0386N using 2000 km long cross sections spaced at 50 km increments from Kilauea Volcano (where the hotspot is hypothesized to be centered) to the bend in the Hawaii-Emperor seamount change (Fig. 5).

Bathymetric features that unrelated to the Hawaiian swell which persist through filtering and are of consequence for our analysis include the Hess Rise and the Mid-Pacific Mountains. The Hess Rise, dated to 98 – 110 Ma [Pringle & Dalrymple, 1993], is situated northeast of the Hawaiian-Emperor bend (Fig. 1, 5). Filtered topography of the Hess Rise is observed in the northern end of profiles sampled at distances of 2250 to 3500 km from the hotspot center (Fig. 7E, F). The Mid-Pacific Mountains, dated to 123 – 132 Ma [Arnaud-Vanneau & Sliter, 1995; Jenkyns, 1995; Jenkyns et al., 1995; Pringle & Duncan 1995], are broadly observed southwest of the Hawaiian Ridge (Fig. 1, 5). Filtered topography of the Mid-Pacific Mountains is observed in the southern end of profiles sampled at distances of 450 to 3000 km from the hotspot center (Fig. 7C, D, E). In order to avoid interference from these and other non-swell-related features that remain in the bathymetry after filtering, such as the larger Hawaiian Islands and seamounts along the central axis, we identify a visually-determined portion of each profile to highlight pristine swell flanks (Fig. 5, 6, 7). The portions of the filtered cross-sections, which we use to constrain buoyancy flux, are outlined in bold black on Figures 5, 6, and 7. With the signal of the swell adequately isolated, we constrain the buoyancy flux of the plume by identifying the range of fluxes that adequately reproduce the observed swell width and height along each bathymetric transect.

3.2 Analyzing Swell Dimensions for Plume Buoyancy Flux

To relate the changing dimensions of the swell to the buoyancy flux of the plume, we first identify common variables between the equations for swell size and buoyancy flux. The buoyancy flux of the plume is given by

$$B = Q\rho_0\alpha\Delta T \tag{10}$$

The expressions for the length scales L_0 and S_0 share the terms for plume volume flux (Q) and plume excess temperature (ΔT) with buoyancy flux. Therefore, to predict the bathymetric response

to changes in buoyancy flux, we can vary plume volume flux and excess temperature to produce a range of swell dimensions.

To compare the range of predicted swell dimensions to the filtered bathymetry, we utilize the swell profile equation of Wessel [1993], who concluded that a super-Gaussian function such as $S = He^{-\left|\frac{y}{W}\right|^5}$ best replicated the steep flanks and flat top of swell bathymetry. To integrate our predicted dimensions into the Wessel [1993] equation, the height of the swell (H) is represented by our equation for swell amplitude $H(t)$ (Eq. 6), while the profile half width (W) is similarly replaced by our expression for swell half width ($L(t)$) (Eq. 1). By systematically examining a range of plume excess temperatures (ΔT) and material fluxes (Q), we produce a series of predicted profiles using Wessel's [1993] equation, and compare these profiles to cross-sections of the filtered swell topography of the same age (Fig. 6, 7).

To minimize uncertainty in the position of the central axis of the swell and ensure the best fit between the modeled and sampled swell profiles, the center point of the modeled profile is allowed to vary along the transect by 100 kilometers in each direction from the center. Even in cases where only one flank of the swell is chosen for comparison, the center point of the swell is still allowed to vary to improve the model fit, under the assumption that the swell center should be close to the plume axis. Chosen profile center points are labeled on figure 5 as white diamonds. To grade the fit of predicted swell dimensions to the bathymetry, we compute the least squares difference between the sampled bathymetry and each modeled profile in meters, resulting in a grid of average profile "misfits" or separation between curves (Fig. 6B). By searching each misfit grid for the minimum error solution, we determine a range of best-fitting values for buoyancy flux of the Hawaiian plume as a function of the age of emplacement over the last 50 million years (Fig. 6C).

4. Constraints on Hawaiian Buoyancy Flux

Our analysis (Fig. 8A) suggests timelines for the buoyancy flux of the Hawaiian plume, associated with the two plate-motion scenarios of O'Connor et al. [2013]. Both buoyancy flux histories show major fluctuations since the bend in the Hawaiian-Emperor Ridge. From 50 to ~25 Ma, buoyancy flux appears to be relatively low, around 3000 $kg\ s^{-1}$, with a steady increasing trend. From 25 to ~10 Ma, our results suggest that Hawaiian buoyancy flux increased exponentially toward a maximum between 12 and 16 Ma, followed by a ~30% decline toward a minimum at 5 Ma. A subsequent ~20% increase brought rates toward their present-day value of about 6000-8000 $kg\ s^{-1}$. Our results suggest that over the last 30 million years the Hawaiian plume has experienced at least a doubling in average flux and that current rates are close to the historical peak that occurred around 15Ma (Fig. 8A).

Compared to previous histories of Hawaiian plume buoyancy flux produced by Davies [1992] and Vidal & Bonneville [2004], our results suggest similar trends since ~45 Ma with some key differences. For example, Davies [1992] suggests an earlier increase to high buoyancy flux than our results (Fig. 8A). We attribute this disparity to the swell delineation and swell magnitude interpretation methods of Davies [1992]. Unlike our own methods of comparing predicted swell dimensions to filtered swell topography, Davies [1992] interprets buoyancy flux from swell dimensions using a rectangular schematic to infer the cross-sectional area of residual swell profiles, isolated visually from the Hess Rise and the Mid Pacific Mountains. We ascribe the early high buoyancy flux of Davies [1992] to over-estimations of swell area caused by the rough rectangular schematic used to infer magnitude from swell dimensions and the inclusion of erroneous features such as the Hawaiian Ridge and the Mid Pacific Mountains.

Vidal & Bonneville [2004] suggest trends in Hawaiian buoyancy flux that are similar to ours since 40 Ma, but with significantly smaller magnitudes (Fig. 8A). Similarities between the two buoyancy

flux trends are attributed to parallel methods used for sampling and dating swell topography. Instead, differences in magnitude result from contrasting methods used to infer buoyancy flux from swell topography. Improving on the methods of Davies [1992], Vidal & Bonneville [2004] constrain buoyancy flux from the cross-sectional area of filtered residual swell topography. However, their method depends strongly on their model for lithospheric subsidence to determine volcanic depth anomalies associated with the islands and seamounts, which greatly impacts the estimated area of the swell. For example, using the PS [Parsons & Sclater, 1977] subsidence model, Vidal & Bonneville [2004] found a range of buoyancy flux between 500 and 6000 $kg\ s^{-1}$ (Fig. 8A). By contrast, they found a peak buoyancy flux of ~ 4000 $kg\ s^{-1}$ and negative buoyancy flux values for ages greater than ~36 Ma using the GDH1 [Stein & Stein, 1992] subsidence model. Our use of the Hillier & Watts [2005] subsidence model should alleviate this problem because it is specifically appropriate for the Pacific [Zhong et al., 2007], as demonstrated by the near-zero residual bathymetry observed away from the Hawaiian swell and other uplifted Pacific bathymetry (Figure 5, 7).

We can gather additional insight into the impact of our swell analysis method by comparing present-day buoyancy flux rates inferred from a variety of studies of the Hawaiian plume. For example, Asaadi et al. [2011] inferred a buoyancy flux rate of 5610 $kg\ s^{-1}$ from their lubrication theory model that matches the Hawaiian bathymetry. While just below our suggested range of about 5800-7800 $kg\ s^{-1}$ (Fig. 9), we associate two particular differences between our analyses to explain the discrepency. First, we assume a slightly faster recent Pacific plate velocity of 87-108.5 $km\ Myr^{-1}$ (Fig. 3B), versus 85.2 $km\ Myr^{-1}$ used by Asaadi et al. [2011]. Faster plate motions require higher plume buoyancy flux in order to produce the same swell topography, so we expect our results to yield higher buoyancy flux because we assume a faster plate velocity. Second, our analysis ends at 1 Ma because we use the Asaadi et al. [2011] scaling equations for swell spreading, which are not applicable close to the plume center.

Buoyancy flux measurements for present day obtained using a geometric analysis method [e.g. Davies, 1988; Sleep, 1990; King & Adams, 2014] tend to suggest buoyancy flux rates of about 5000-9000 $kg\,s^{-1}$, which span a wider range than our estimate between 6000-8000 $kg\,s^{-1}$ (Fig. 8A). Similar to our earlier comparison to Davies [1992], we attribute these differences in flux values to differences in the way these other studies measured swell dimensions, and thus swell volume, from the residual swell topogrpahy. However, another explanation is that such geometric analyses of swell topography also assume that the plume material supporting the swell is pinned to the lithosphere and do not take into account continued deformation of plume material relative to the plate and its impact on swell topography. This process is built into the Asaadi et al. [2011] scaling equations used here.

Numerical analyses by Ribe & Christensen [1994] suggest present rates of Hawaiian buoyancy flux of 4100 $kg\,s^{-1}$, significantly smaller than our estimates (Fig. 8A). We attribute the smaller buoyancy flux rates from these models to their assumption of Newtonian rheology for the deformation of plume material beneath the lithosphere. Unlike dislocation creep rheology (non-Newtonian) that suggests a stagnation of swell widening after ~3 million years, diffusion creep rheology (Newtonian) suggests continued spreading and a more rapid drop off of swell height [Asaadi et al. 2011]. Because the peak in dynamic topography above the plume is greater for newtonian rehology, a swell governed by Newtonian rheology requires less buoyant material to generate equivalent swell topography near the hotspot center. Thus, Ribe & Christensen's [1994] estimates of lower plume flux likely result from the assumption of Newtonian rheology.

While differing methods of interpretation suggest varying scales of temporal fluctuations in Hawaiian buoyancy flux, it is equally important to understand the scale of fluctuations that our methodology is able to resolve. For the purposes of our analysis, our temporal resolution is governed by the length scale of the swell itself. If we assume that the swell averages plume flux

variations along a length scale comparable to its ~1000 km width and that a typical plate velocity is ~100 $km\ Myr^{-1}$, then the temporal resolution of our model is ~10 million years. This temporal resolution makes it difficult to confidently constrain any shorter-duration fluctuations shown in our results. However, general trends over the 50 million year history of Hawaiian buoyancy flux described in this section should be robust.

5. Discussion

Our results, consistent with the conclusions of Davies [1992] and Vidal & Bonneville [2004], suggest that the buoyancy flux of the Hawaiian mantle plume has changed significantly since the Hawaiian-Emperor Bend (HEB) roughly 50 million years ago (Fig. 8A). Our methodology suggests that the observed fluctuations in Hawaiian buoyancy flux could be caused by changes in either material flux (Q) or plume excess temperature (ΔT), or both. However, because our technique does not allow for the discernment of either Q or ΔT from the overall effect of increased buoyancy flux on the swell, other methods are needed to assess their relative influences independently. Geothermometry may provide an independent constraint on plume excess temperature, which Tree et al. [In Prep] have used to suggest an increase in excess plume temperature of at least a hundred degrees since ~50 Ma. Assuming an increase in ΔT from 300 to 400 degrees, our methods would suggest that an increase in ΔT of only 100 degrees could potentially explain a ~33% increase in buoyancy flux. This suggests the near doubling of buoyancy flux since 50 Ma would require an increase in material flux to accompany the increase in excess temperature. However, it is difficult to determine the relative contributions of changes in excess temperature and material flux during the lifetime of the plume without some additional independent constraints on either of these parameters.

Alternative measurements of plume activity could provide the necessary insight into the changing conditions of the plume. One such measurement of plume activity is melt flux, which is the rate at which volcanic material is erupted onto the surface of the overlying plate. Unlike most buoyancy flux estimates for Hawaii, the melt flux histories suggested by Vidal & Bonneville [2004] imply a continued increase in plume activity through present day (Fig. 8B). By contrast, Van Ark & Lin [2004] suggest a local peak in activity near 2 Ma with slightly lower rates currently (Fig. 8B). Assuming that the production of volcanic material is more closely tied to plume excess temperature than material flux [e.g. Ribe & Christensen, 1999; Farnetani & Hofmann, 2010], the melt flux estimates of Vidal & Bonneville [2004] would suggest that the increase in plume activity since ~50 Ma is primarily associated with an increase in plume excess temperature. Alternatively, the decreased melt flux estimates of Van Ark & Lin [2004] would suggest that the recent increase in buoyancy flux can be attributed to changes in both material flux and temperature. However, without further constraints on the link between plume properties and the generation of extrusive volcanic material, it is difficult to further constrain our history of Hawaiian buoyancy flux using estimates of melt flux.

Another possible explanation for variations in the estimation of plume buoyancy flux from measurements of the swell could be related to motion of the plume conduit beneath the lithosphere. Much like changes in the velocity of the Pacific plate, lateral motion of the plume changes the relative plate velocity, alters the accumulation of plume material, and therefore changes the interpretation of buoyancy flux. One example of possible plume motion, by Tarduno et al. [2009], suggests a 'plume whip' scenario in which the plume head was captured by a divergent margin, pulled away from the source in the lower mantle by plate motion, and later released to 'whip' back to a vertical orientation over the source. Without discounting the plume motion scenario of Tarduno et al. [2009], our methods would suggest that plume motion is not responsible for the increase in interpreted buoyancy flux since ~50 Ma because motion of the plume is already included in our

analysis through the O'Connor et al. [2013] age progressions. Because O'Connor et al. [2013] based their plate velocity progressions off of the volcanic ages along the Hawaiian Ridge, their velocities express motion of both the plume and the plate, since the formation of the volcanoes is representative of the positon of the plume beneath the lithosphere.

Despite our improved method for constraining plume buoyancy flux, uncertainty in our estimates remains. At the base our method, some uncertainty is associated with the Asaadi et al. [2011] scaling equations used to predict the evolution of swell dimensions, particularly near the plume where the swell scaling equations (equations 1-3) differ from their lubrication theory solution for the deformation of Non-Newtonian plume material. Uncertainty is also associated with our implementation of variations in relative plate velocity in our method. First, the progressions of relative plate velocity models suggested by O'Connor et al. [2013] include inherent uncertainty. Without constraints on the possible motions of either the Pacific plate or the plume, the 'single shift' linear progressions chosen by O'Connor et al. [2013] to fit the geochemical ages of the Hawaiian-Emperor ridge induces some uncertainty into our interpretation of buoyancy flux variations. Second, our use of an averaged term of apparent velocity, $\langle U \rangle$, to represent the continuous spreading of the sub-lithospheric swell, is a simplified representation of a more complex process; this suggests some uncertainty is associated with the interpretation of evolved swell dimensions. However, much like the Asaadi equations, without constraints on the uniqueness of the O'Connor et al. [2013] velocity progressions, or constraints on the deformation rates of the ponding plume material, quantifying this uncertainty remains a challenge.

Nevertheless, we can visualize uncertainty associated with our interpretation of relative plate velocity by comparing buoyancy flux curves based on different progressions for plate velocity (Fig. 9). Using the plate velocity progressions of O'Connor et al. [2013], the assumption of an instantaneous response of the deforming plume head to a change in relative plate velocity (that is,

assuming that $\langle U \rangle = U$ in our analysis), suggests step-function changes in buoyancy flux at either 17 or 27 Ma, with significantly decreased rates of buoyancy flux prior to the jump (Fig. 9). Assuming an average constant plate velocity of 75 $km\,Myr^{-1}$, intermediate between the 59-108.5 $km\,Myr^{-1}$ rates suggested by the O'Connor et al. [2013] analysis (Fig. 3B), suggests Hawaiian buoyancy flux increases from 50 Ma to peak at ~7000 $kg\,s^{-1}$ around 17 Ma and slowly declines through 10 Ma to ~5000 $kg\,s^{-1}$ (Fig. 9). Differences between these models give an indication for how our treatment of plate velocity changes affect our estimates for the time history of buoyancy flux. The similarity in trends, particularly for times earlier than ~20 Ma, supports our conclusion that plume buoyancy flux gradually doubled between 50 and 20 Ma (Fig. 9).

Two final sources of uncertainty in our measurements stem from the dimensional comparison method we use to constrain buoyancy flux. First, while different combinations of plume material flux (Q) and excess temperature (ΔT) create similar sets of predicted swell profiles, the values of buoyancy flux associated with those couplings of Q and ΔT are not unique. Therefore, when a set of predicted swell dimensions is determined as the solution, the associated value of buoyancy flux is not unique to those dimensions of the swell, and suggests instead a range of buoyancy flux values around the misfit of the solution. The second source of uncertainty, one outlined by King & Adams [2014], is that characterization of the swell signal through geometric comparison includes inherent and unquantifiable error stemming from the variability in swell shape. Unlike the idealized swell profile of Wessel [1993], the observed swell does not always conform to a specific geometric shape. Uncharacterized variations in the plume or plate result in a truly unique swell form that may evolve along the length of the swell. Therefore, analyzing swell dimensions using a standardized geometric profile introduces uncertainty into the assessment of swell magnitude; King & Adams [2014] suggested that such unquantifiable uncertainty in the analysis method can be gauged by variability in

the results. To account for the uncertainty in our measurements of Hawaiian buoyancy flux, we included a region of 25% variability within the range of possible buoyancy flux (Fig. 8A).

6. Conclusions

To improve upon previous estimates of Hawaiian plume buoyancy flux, we developed a swell analysis model that predicts swell topography in order to constrain variations in buoyancy flux. We have shown that swell topography can be highlighted and identified beyond initially assumed bounds by removing the bathymetric signals of ocean sediments and lithospheric subsidence, and filtering out short wavelength signals such as islands and seamounts not associated with the formation of the swell. We have also shown that estimates of buoyancy flux can be improved by assuming a Non-Newtonian rheology for the deformation of plume material, and by accounting for fluctuations in swell dimensions associated with changes in relative plate motion and thermal subsidence.

Applying our methodology to 73 cross-axial profiles of isolated swell topography, we have constrained variations in Hawaiian plume buoyancy flux since ~50 Ma. Our swell reconstruction model suggests that the average buoyancy flux of the Hawaiian plume has more than doubled since ~30 Ma, and has exhibited fluctuations of ~ 30% since 15 Ma. The temporal resolution of our results scale with swell width, which suggests that our method can resolve variations in plume buoyancy flux occurring over timescales of ~10 million years. Uncertainty in our method arises from the scaling equations used to predict swell evolution, uncertainty in the history of relative plate velocity, and the comparison between our predicted swell dimensions and the isolated swell topography.

Comparisons between our results and previous histories of Hawaiian plume buoyancy flux created by Davies [1992] and Vidal & Bonneville [2004], show similar trends with some key differences. Davies [1992] suggests similar variations and overall values for historical buoyancy flux,

but the ages for key shifts in flux do not agree. We attribute the differences between our estimates and those of Davies [1992] to inaccurate estimates of swell dimensions stemming from inadequately isolated swell topography and the use of a volumetric equation to estimate swell magnitude. Compared to the results of Vidal & Bonneville [2004], our results suggest similar plume flux variations for times after ~20 Ma, but we estimate much larger buoyancy flux rates prior to 20 Ma. We attribute the difference between to the sensitivity of Vidal & Bonneville's [2004] method to their choice of a lithospheric subsidence model.

From our analysis of the swell, we suggest that the variations in Hawaiian plume buoyancy flux can be attributed to changes in either the material flux (Q) or excess temperature (ΔT) of the plume, or both. However, without independent constraints on either qualities of the plume, discerning the relative contributions of these two plume attributes is difficult. We can be confident that our inferred variations in plume buoyancy flux are not apparent changes associated with motion of the plume, because we include constraints on plume motion relative to the plate as part of our analysis [O'Connor et al., 2013]. Thus, the doubling of buoyancy flux from the Hawaiian plume between 30–50 Ma and 0–20 Ma must be due to a deep mantle process that causes a sustained increase in the volume or excess temperature of material passing through the Hawaiian plume.

Figures

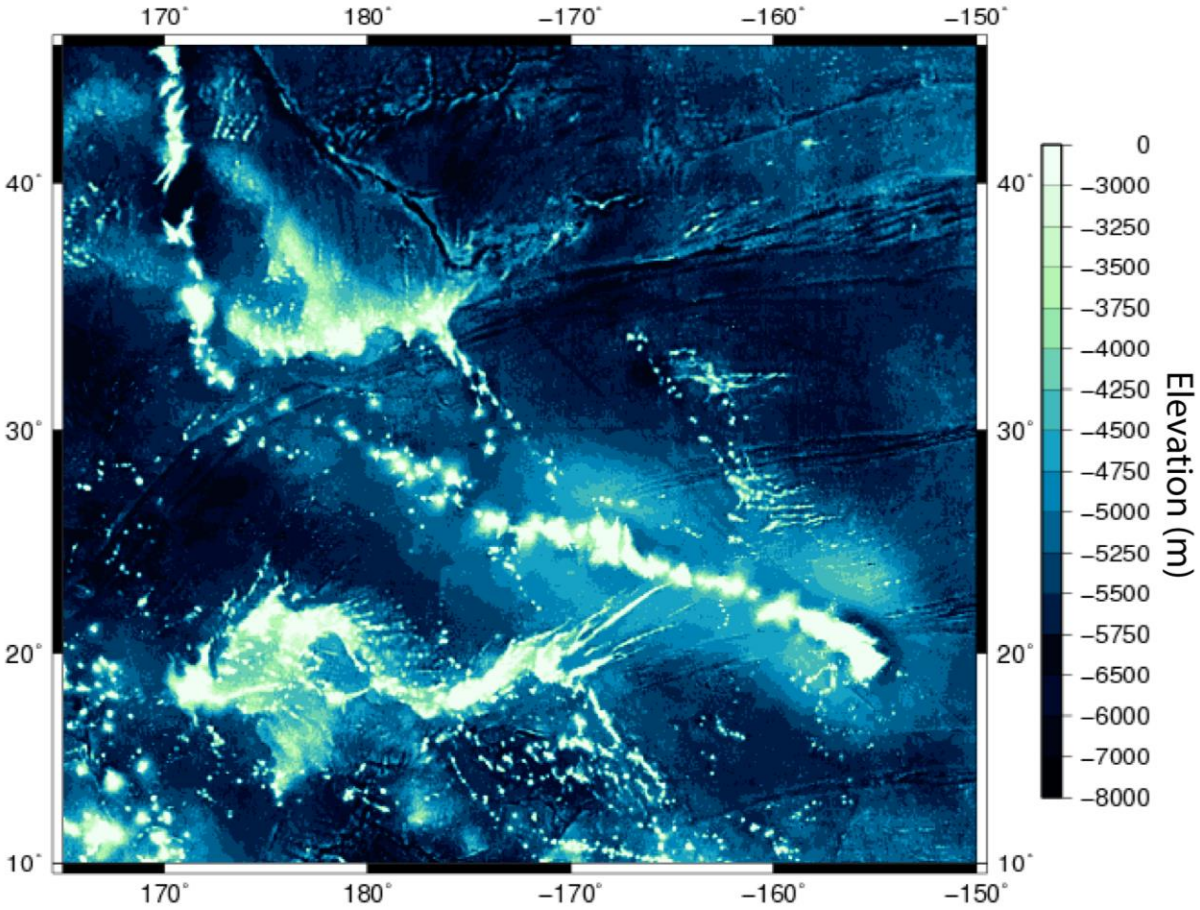

Figure 1: Elevation of the Hawaiian Ridge across the central Pacific. Shallow swell topography (broad light blue colored region) surrounds the Hawaiian Ridge.

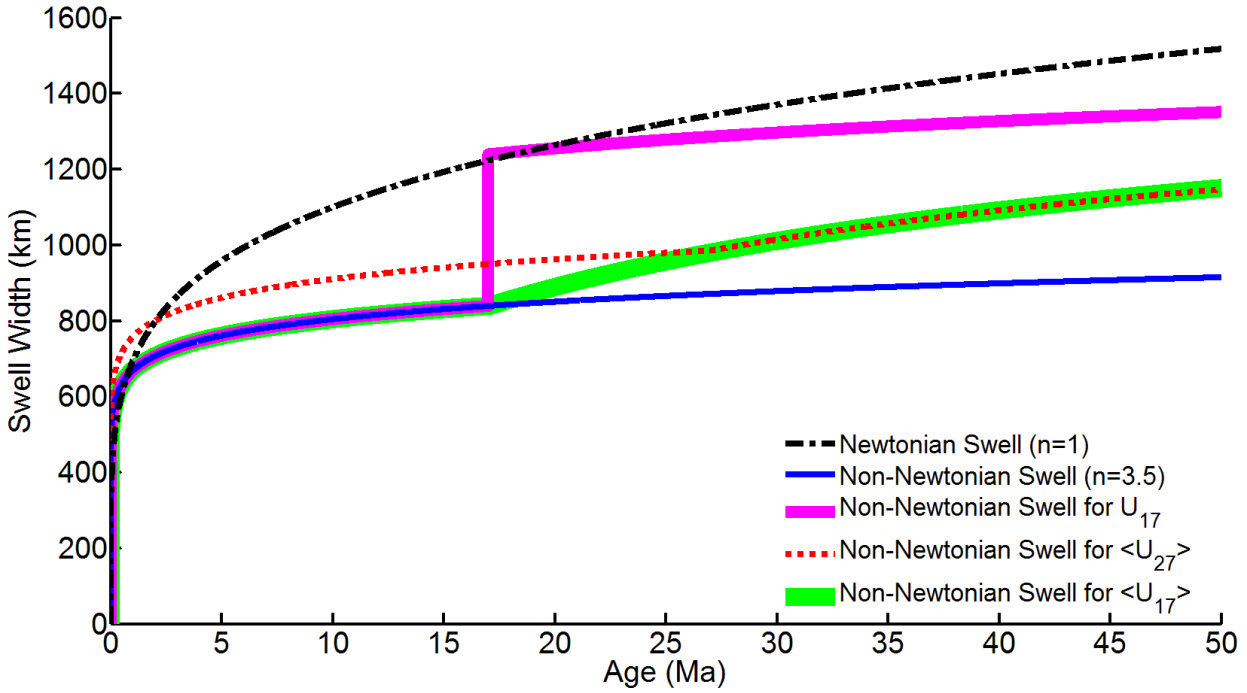

Figure 2: Changes in the Rate of Swell Widening can reflect either a difference in plume rheology or a change in plate velocity relative to the plume location, assuming constant buoyancy flux (we use 10,710 $\boldsymbol{kg\ s^{-1}}$ for the curves shown here). Adjusting these variables in the Asaadi et al. [2011] equation for swell widening, allows us to visualize the impact each variable on the development of the swell. As a control case for swell widening a Newtonian plume spreading beneath a plate that does not change velocity shows the greatest rate of sustained widening of the swell (black dash-dot line). Reproducing the swell progression of Asaadi et al. [2011], without a shift in plate velocity, emphasizes the decreased efficiency of swell widening associated with Non-Newtonian rheology (blue solid line). Including an increase in plate velocity relative to the plume location, as suggested by O'Connor et al. [2013] for the Pacific plate moving over the Hawaiian Plume, (Fig. 3B), shows that the increase in plate velocity tends to narrow the swell. Implementing this velocity increase using the Asaadi et al. [2011] equations directly predicts a sharp change in swell width (pink line), while accounting for a more gradual response of swell spreading produces a slower change in width (red dotted and green solid lines).

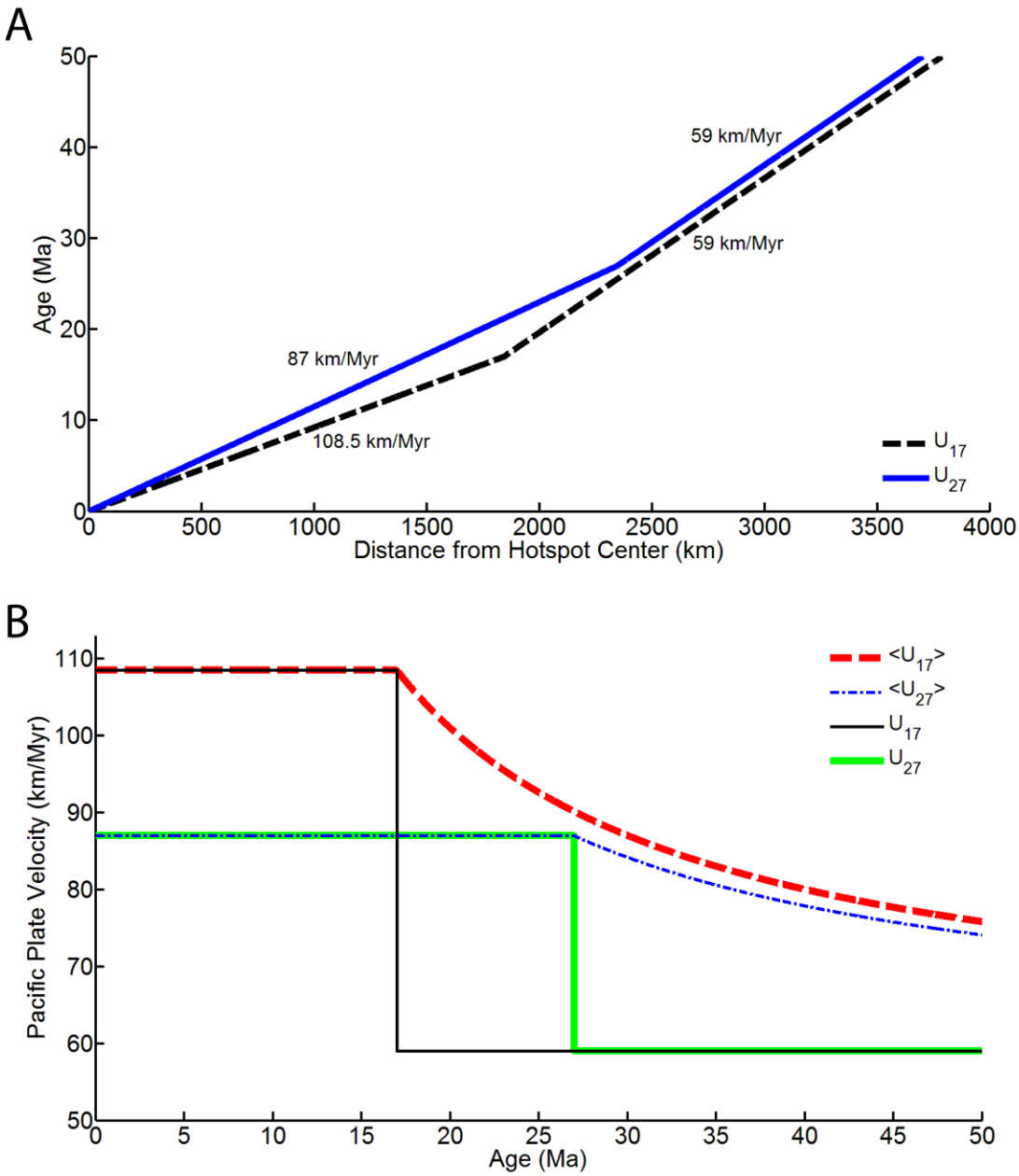

Figure 3: Velocity of the Pacific Plate relative to the Hawaiian plume conduit has changed significantly since the Hawaiian-Emperor Bend roughly ~50 million years ago. [**A**] Based on the progression of Hawaiian volcanism, O'Connor et al. [2013] suggests two possible histories for relative plate velocity near Hawaii. Because the velocity of the plate is measured from the ages of the islands and seamounts along the Hawaiian ridge, the velocity progressions suggested by O'Connor et al. [2013] account for both changes in the rate of plate motion near Hawaii as well as any motion of the plume head itself. [**B**] Relative Pacific plate velocity models proposed by O'Connor et al. [2013] (solid lines) and the average relative velocity of the plate from the time of eruption to the present (dashed and dash-dot lines), which is relevant for computing the spreading rate of deforming plume material.

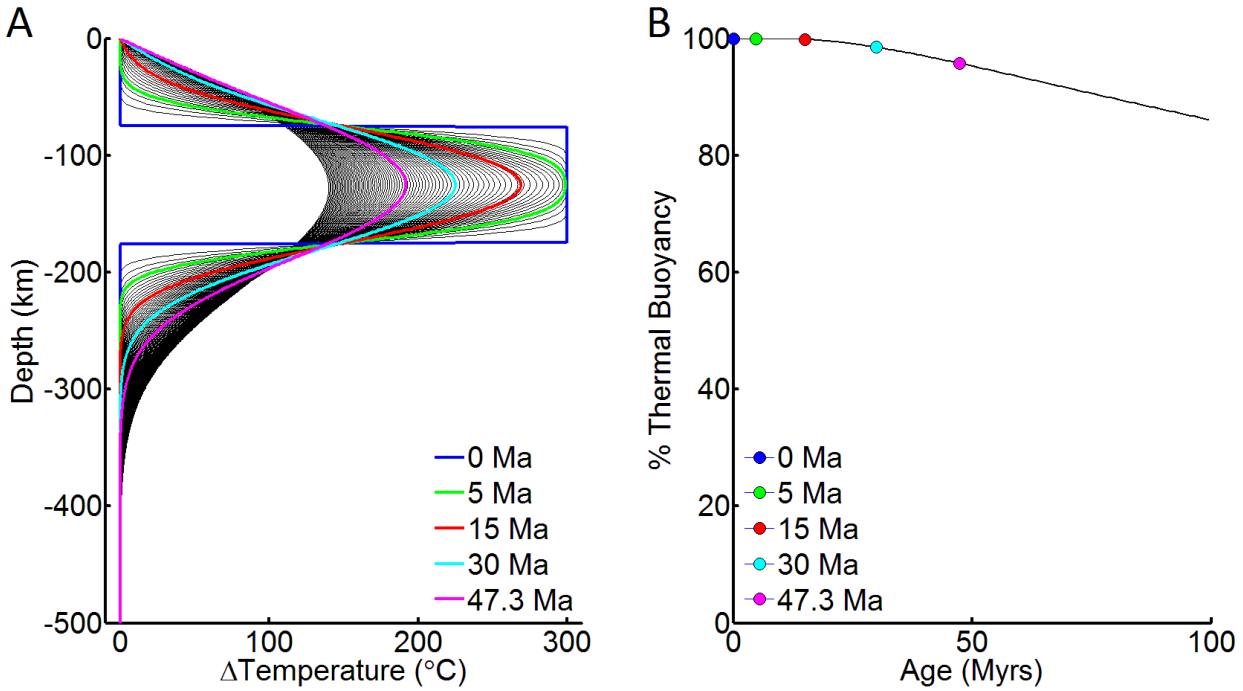

Figure 4: Evolution of Plume Excess Temperature and Thermal Buoyancy. [**A**] Profiles of evolving excess temperature show that, over time, thermal diffusion distributes the temperature anomaly of the plume between the lithosphere (above) and the ambient mantle (below). [**B**] Total thermal buoyancy of the lithosphere and plume, which determines the isostatic support of the topographic swell, as a function of age. Heat remains in the lithosphere-plume-mantle system until it is lost through the surface. Over the ~50 Ma lifetime of the Hawaiian swell, only about 5% of the plume's thermal buoyancy is lost.

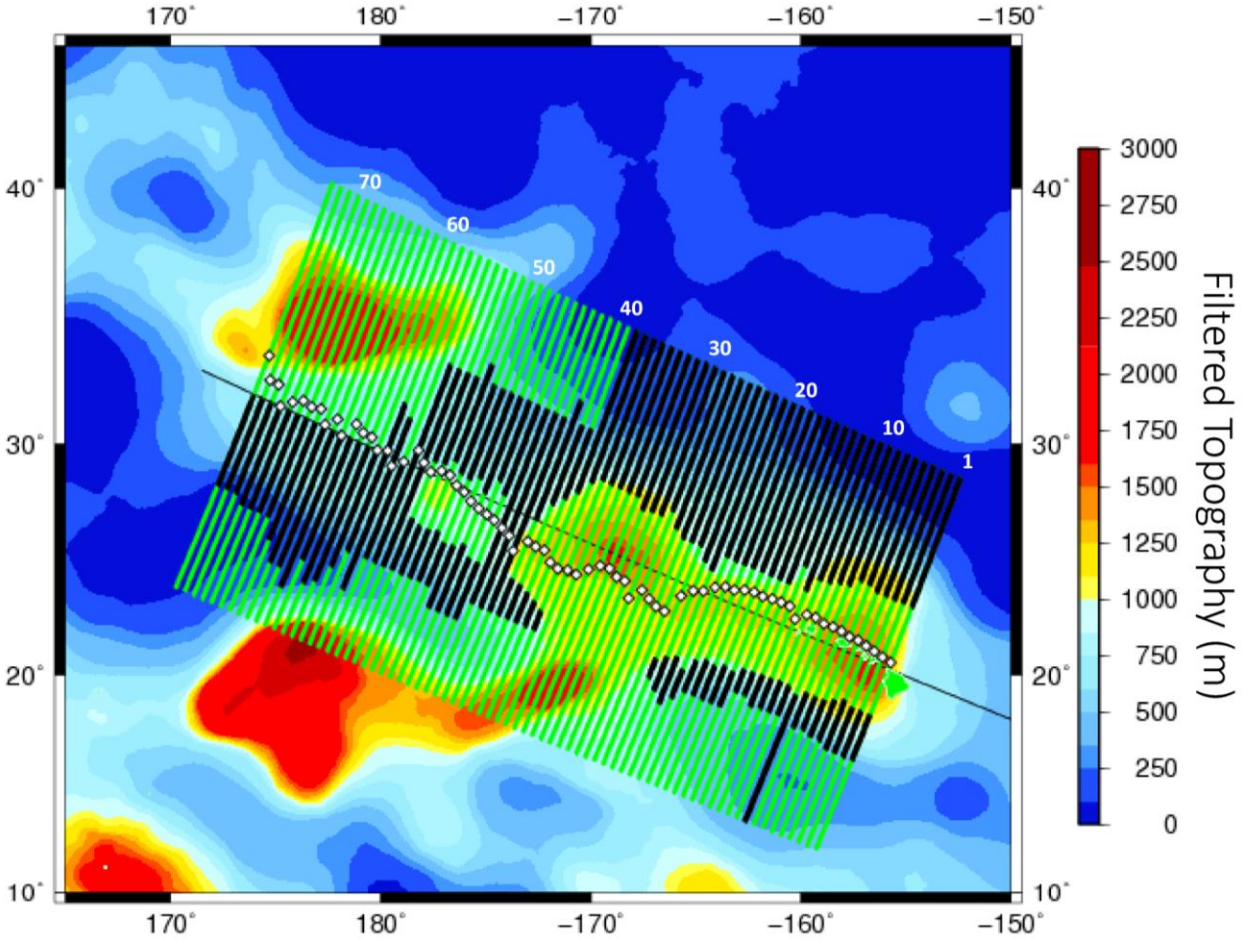

Figure 5: Sampling Filtered Swell Topography. The filtered signal of the swell is sampled 73 times across the Hawaiian Ridge for buoyancy flux analysis (green solid lines). Subsets of each profile are selected for comparison to modeled swell profiles (bold black lines); unselected portions (green lines) are excluded from the comparison because they include topography not associated with the swell. Agreement between modeled swell profiles and cross-sections of filtered bathymetry is improved by allowing the center point of the swell (white diamonds) to vary within 100 kilometers to either side of the interpreted sample track (thin solid black line)

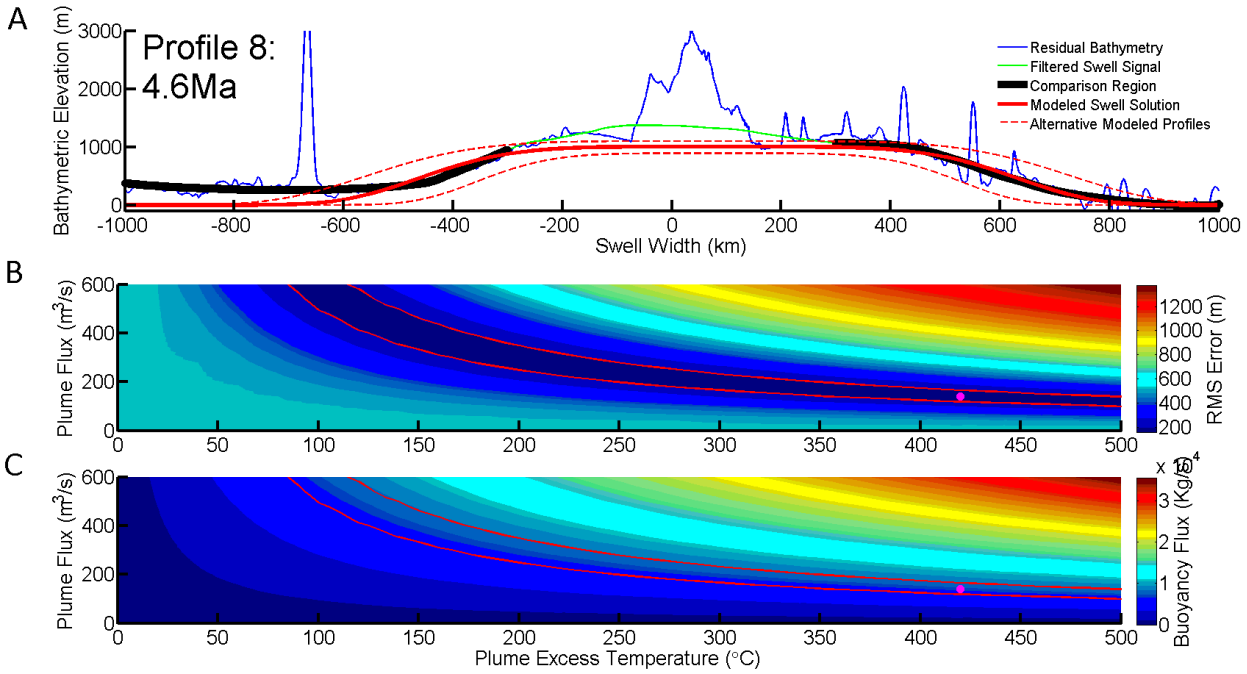

Figure 6: Buoyancy Flux Analysis of the Hawaiian Swell at 4.6 Ma. [**A**] A comparison of residual bathymetry (blue line) and filtered bathymetry (green line, with the comparison region highlighted with thick black line) to modeled swell bathymetry (red line) for a cross section of the Hawaiian swell at 4.6 Ma (see Fig. 5). [**B**] The root mean square (RMS) difference between the modeled swell bathymetry and the filtered swell bathymetry as a function of plume flux and plume excess temperature, for the selected comparison region (black line in A, also shown in Fig. 5). Combinations of plume flux and excess temperature that produce RMS values within 25% of the minimum value (shown by the pink dot) are bounded by red lines. [**C**] Buoyancy flux of the plume as a function of plume flux and plume excess temperature, with the region of best-fitting solutions from (B) bounded by red lines.

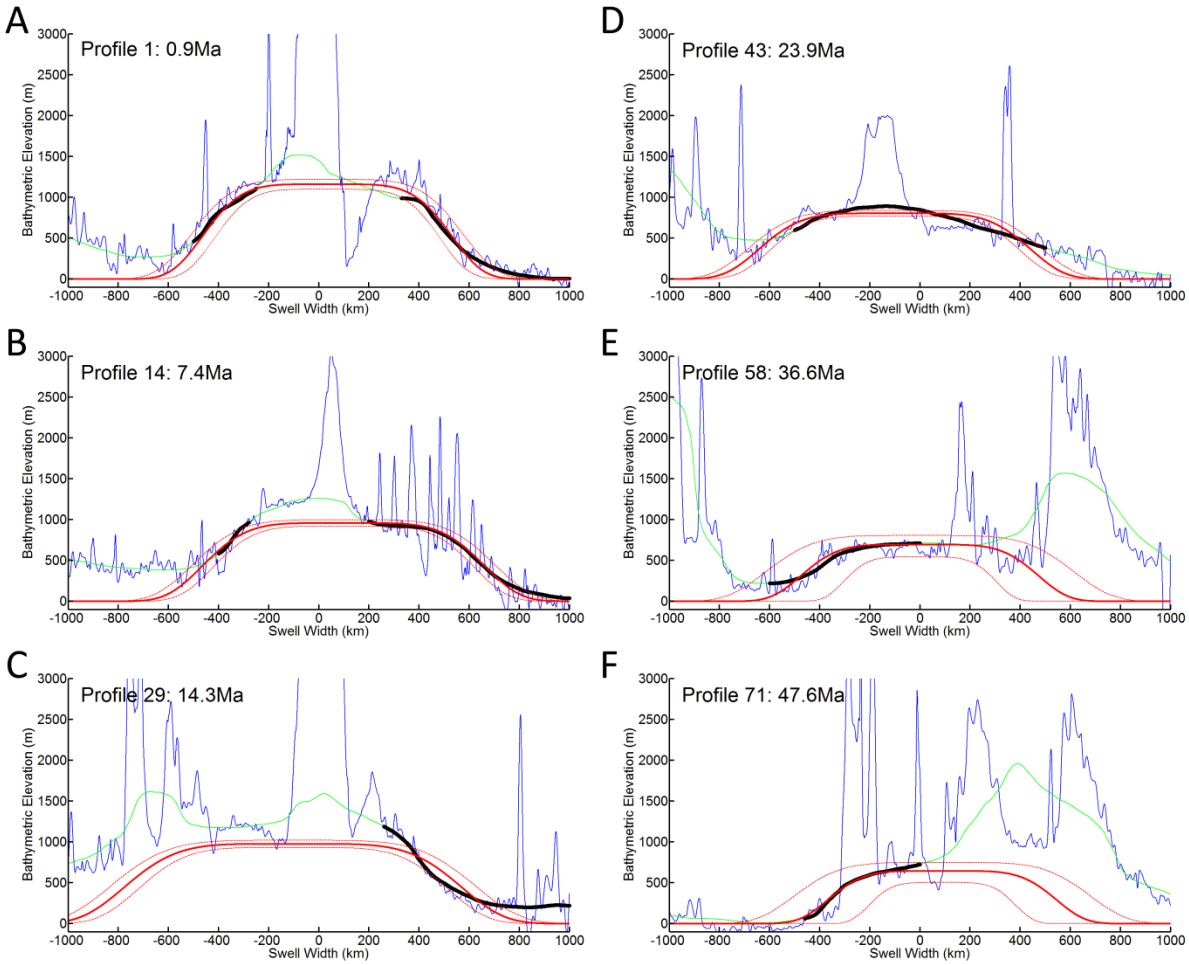

Figure 7: Buoyancy Flux Analysis from the hotspot to the HEB. Comparison regions between modeled swells and the filtered swell profiles, with line colors and styles given by Fig. 6A. Here we show how only the swell-induced variations in bathymetry are used to constrain buoyancy flux (thick black lines). [**A**, **B**] For segments of the swell within the Hawaiian Archipelago both flanks of the swell are selected, leaving out the bathymetric highs associated with the islands. [**C**, **D**] Further along the swell where the Mid-Pacific Mountains (MPM) begins to intrude into profiles of the swell, the east flank of the swell is selected for comparison. In some cases where there is only a small anomaly for the island or seamount, the swell platform is also selected. [**E**, **F**] Toward the end of the swell, near the HEB, swell topography is shrouded by the Hess Rise to the East, and the west flank of the swell is selected for comparison.

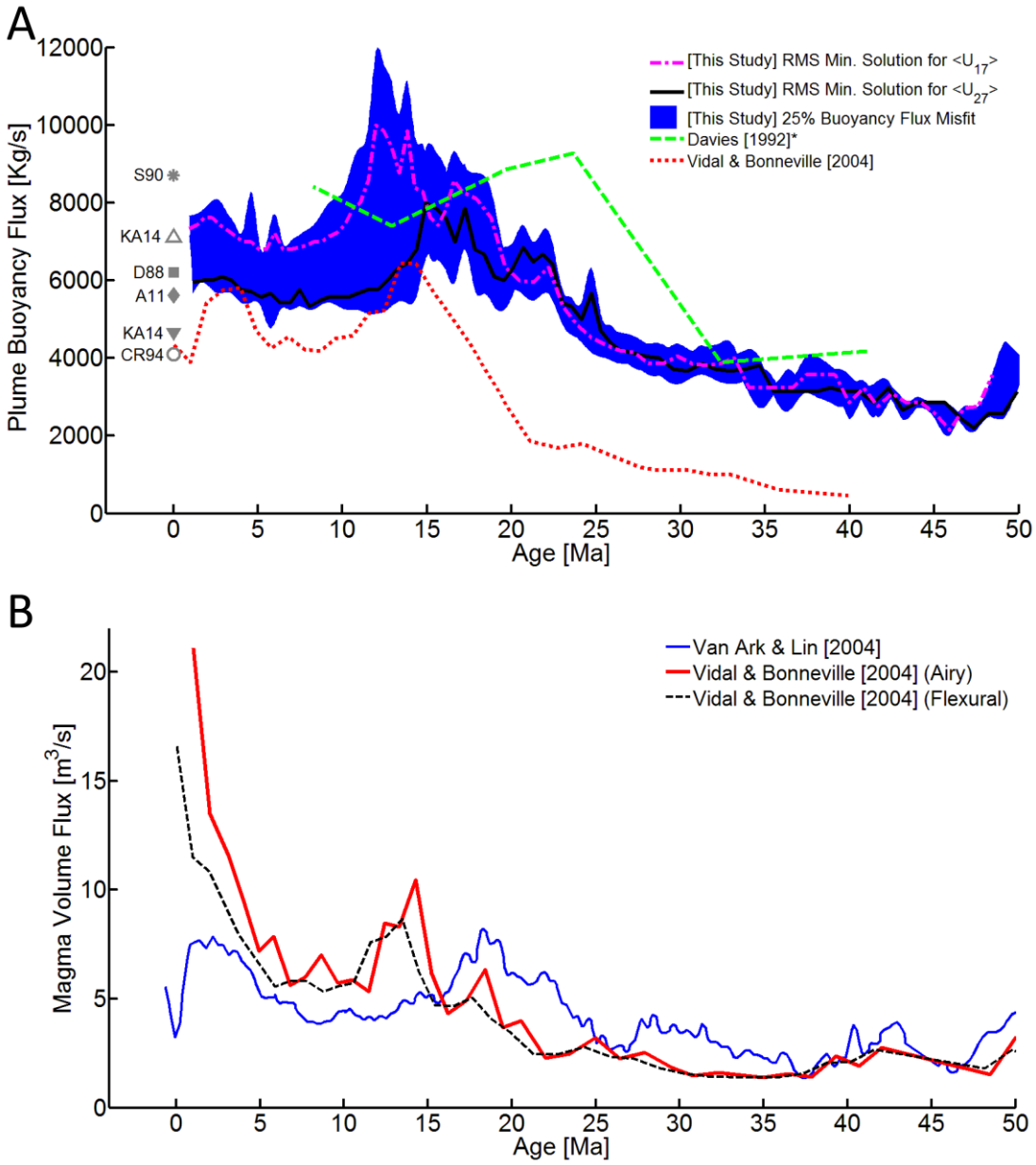

Figure 8: Temporal Variations in Hawaiian Plume Buoyancy Flux and Magma Volume Flux. [**A**] Analysis by Vidal and Bonneville [2004] (dotted red line), Davies [1992] (dashed green line), and our own study (solid black and dash-dot pink lines) suggest major variations in Hawaiian plume buoyancy flux since 50 Ma. To improve the correlation of data sets, the data of Davies [1992] is adjusted to O'Connor et al.'s [2013] age-distance relationship for a shift in plate velocity at 17 Ma. Misfit for our study (blue filled area), estimated here as buoyancy flux values with analyzed RMS values within 25% of the minimum error solution for either curve, represents uncertainty in our analysis induced by our dimensional analysis method, the integration of the O'Connor et al. [2013] progressions for apparent Pacific Plate velocity, and the Asaadi et al. [2011] scaling equations for swell development. Current Hawaiian buoyancy flux estimates by Sleep [1990] (S90 – star), King & Adams [2014] (KA14 – triangle), Davies [1988] (D88 – square), Asaadi et al. [2011] (A11 – diamond), and Ribe & Christensen [1994, 1999] (CR94 – circle) are represented by symbols at 0 Ma, without age precision given by the authors. The range of suggested current buoyancy flux by King &

Adams [2014] is indicated by open and closed triangles, for the maximum (open) and minimum (closed) vales. [**B**] Similar to the analyses of buoyancy flux in [A], measurements of Hawaiian magma volume flux by Van Ark & Lin [2004] (solid blue line) and Vidal & Bonneville [2004] (dashed black and solid red lines) suggest a major increase in Hawaiian plume activity since 50 Ma.

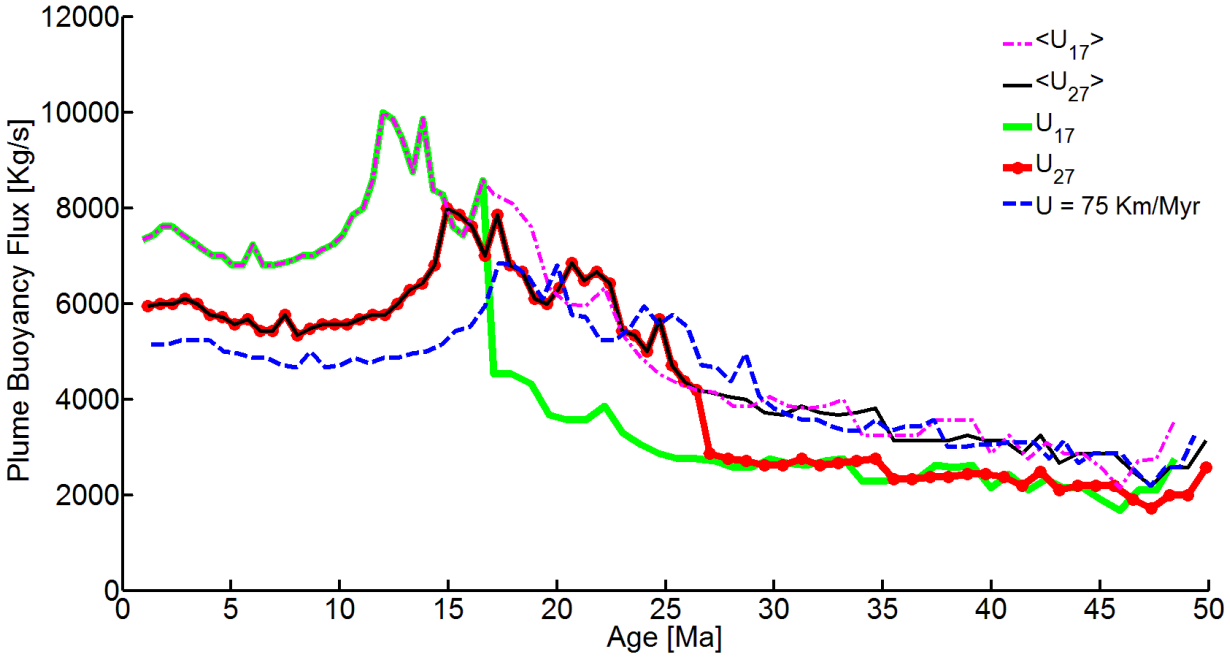

Figure 9: Variations in Buoyancy Flux Measurements caused by Differences in Assumed Plate Velocity. Here we show how different models of relative Pacific Plate velocity affect our interpretation of Hawaiian buoyancy flux. The resultant histories from our analysis assuming averaged progressions for plate velocity are reproduced from Figure 8 as $\langle \boldsymbol{U_{17}} \rangle$ (pink dash-dot line) and $\langle \boldsymbol{U_{27}} \rangle$ (solid black line). Buoyancy flux histories assuming an instantaneous shift in plate motion are shown for both O'Connor et al. [2013] relative plate velocity progressions as $\boldsymbol{U_{17}}$ (bold green line) and $\boldsymbol{U_{27}}$ (solid red line with circle markers), and suggest dramatically lower values of buoyancy flux before the changes in plate velocity at 17 and 27 Ma. A history of Hawaiian buoyancy flux is also shown for the assumption of a constant velocity plate as $\boldsymbol{U = 75\ km\ Myr^{-1}}$ (dashed blue line), and suggests similar trends in buoyancy flux through ~20 Ma with decreased rates through the present.

References

Asaadi, N., Ribe, N. M., & Sobouti, F. (2011). Inferring nonlinear mantle rheology from the shape of the Hawaiian Swell. *Nature , 473* (7348), pp. 501-503.

Amante, C. and B.W. Eakins (2009). ETOPO1 1 Arc-Minute Global Relief Model: Procedures, Data Sources and Analysis. NOAA Technical Memorandum NESDIS NGDC-24. National Geophysical Data Center, NOAA. doi:10.7289/V5C8276M [09/21/2012].

Arnaud-Vanneau, A., and Sliter, W.V. (1995). Early Cretaceous shallow-water benthic foraminifers and fecal pellets from Leg 143 compared with coeval faunas from the Pacific Basin, Central America, and the Tethys. *In* Winterer, E.L., Sager, W.W., Firth, J.V., and Sinton, J.M. (Eds.), *Proc. ODP, Sci. Results,* 143: College Station, TX (Ocean Drilling Program), 537–564.doi:10.2973/odp.proc.sr.143.252.1995

Ballmer, M. D., Ito, G., van Hunen, J., & Tackley, P. J. (2011). Spatial and temporal variability in hawaiian hotspot volcanism induced by small-scale convection. *Nature Geoscience Letters*.

Crough, T. S. (1983). Hotspot Swells. *Annual Review of Earth and Planetary Sciences* , 165-193.

Davies, G. F. (1988). Ocean Bathymetry and Mantle Convection: Large-Scale Flow and Hotspots. *Journal of Geophysical Research , 93* (B9), 10467-10480.

Davies, G. F. (1992). Temporal Variation of the Hawiian plume flux. *Earth and Planetary Science Letters , 113* (1-2), 277-286.

Divins, D.L., Total Sediment Thickness of the World's Oceans & Marginal Seas, NOAA National Geophysical Data Center, Boulder, CO, 2003.

Farnetani, C. G., & Hofmann, A. W. (2010). Dynamcs and internal structure of the Hawaiian Plume. *Earth and Planetary Science Letters*, 231-240.

Hillier, J. K., & Watts, A. B. (2005). Relationship between depth and age in the North Pacific Ocean. *Journal of Geophysical Research , 110*, B02405.

Jenkyns, H.C., 1995. Carbon-isotope stratigraphy and paleoceanographic significance of the Lower Cretaceous shallow-water carbonates of Resolution Guyot, Mid-Pacific Mountains. *In* Winterer, E.L., Sager, W.W., Firth, J.V., and Sinton, J.M. (Eds.), *Proc. ODP, Sci. Results,* 143: College Station, TX (Ocean Drilling Program), 99–104. doi:10.2973/odp.proc.sr.143.213.1995

Jenkyns, H.C., Paull, C.K., Cummins, D., and Fullagar, P.D., 1995. Strontium-isotope stratigraphy of lower cretaceous atoll carbonates in the Mid-Pacific Mountains. *In* Winterer, E.L., Sager, W.W., Firth, J.V., and Sinton, J.M. (Eds.), *Proc. ODP, Sci. Results,* 143: College Station, TX (Ocean Drilling Program), 89–97. doi:10.2973/odp.proc.sr.143.212.1995

King, S. D., & Adam, C. (2014). Hotspot swells revisited. *Physics of the Earth and Planetary Interiors , 235*, 66-83.

Li, X., King, R., Yuan, X., Wolbern, I., & Winfried , H. (2004). Rejuvenation of the lithosphere by the Hawaiian plume. *Nature , 427* (6977), 827-829.

Moore, W. B., Schubert, G., & Tackley, P. (1998). Three-Dimensional Simulations of Plume-Lithosphere Interaction at the Hawaiian Swell. *Science* , *279*, 1008-1011.

Morgan, W. J. (1971). Convection Plumes in the Lower Mantle. *Nature* , *230* (5288), pp. 42-43.

O'Connor, J. M., Steinberger, B., Koppers, A. A., Wijbrans, J. R., Haase, K. M., Stoffers, P., et al. (2013). Constraints on past plate and mantle motion from new ages for the Hawaiian-Emperor Seamount Chain. *Geochemistry, Geophysics Geosystems , 14* (10), 4564-4584.

Olson, P. (1990). Hot spots, swells and mantle plumes. In M. P. Ryan (Ed.), *Magma Transport and Storage* (pp. 33-51). New York: John Wiley.

Parsons, B., & Sclater, J. (1977). An analysis of the variation of ocean floor bathymetry and heat flow with age. *Journal of Geophysical Reserach , 82* (5), 803-827.

Pringle, M. S., & Dalrymple, G. B. (1993). Hess Rise, Wentworth Seamount Chain. In *The Mesozoic Pacific: Geology, Tectonics and Volcanism* .

Pringle, M.S., and Duncan, R.A., 1995. Radiometric ages of basaltic lavas recovered at Sites 865, 866, and 869. *In* Winterer, E.L., Sager, W.W., Firth, J.V., and Sinton, J.M. (Eds.), *Proc. ODP, Sci. Results,* 143: College Station, TX (Ocean Drilling Program), 277–283. doi:10.2973/odp.proc.sr.143.218.1995

Ribe, N.M., & Christensen, U. R.(1999). The dynamical origin of Hawaiian Volcanism. *Earth and Planetary Science Letters , 171* (4), 517-531.

Ribe, N.M., & Christensen, U. R. (1994). Three-dimensional modeling of plume-lithosphere interaction. *Journal of Geophysical Research , 99* (B1), 669-681.

Ribe, N. M. (2004). Through thick and thin. *Nature , 427*, pp. 793-795.

Sleep, N. H. (1990). Hotspots and Mantle Plumes: Some Phenomenology. *Journal of Geophysical Research , 95* (B5), 6715-6736.

Stein, C., & Stein, S. (1992). A model for the global variation in oceanic depth and heat flow with lithospheric age. *Nature , 359*, 123-129.

Steinberger, B., & Antretter, M. (2006). Conduit diameter and buoyant rising speed of mantle plumes: Implications for the motion of hot spots and the shape of plume conduits . *Geochemistry Geophysics Geosystems , 7* (11).

Steinberger, B., & O'Connell, R. J. (1998). Advection of plumes in mantle flow: implications for hotspot motion, mantle viscosity and plume distribution. *Geophysical Journal International , 132* (2), 412-434.

Sykes, T. J. (1996). A correction for sediment load upon the ocean floor: Uniform versus varying sediment density estimations-implications for isostatic correction. *International Journal of Marine Geology, Geochemsitry and Geophysics , 133* (1-2), 35-49.

Tarduno, J. A., Duncan, R. A., Scholl, D. W., Cottrell, R. D., Steinberger, B., Thordarson, T., et al. (2003). The Emperor Seamounts: Southward Motion of the Hawaiian Hotspot Plume in Earth's Mantle. *Science , 301*, pp. 1064-1069.

Tarduno, J., Bunge, H.-P., Sleep, N., & Hansen, U. (2009). The Bent Hawaiian-Emperor Hotspot Track: Inheriting the Mantle Wind. *Science , 324*, pp. 50-52.

Turcotte, D. L., & Schubert, G. (2002). *Geodynamics* (2nd ed.). Cambridge: Cambridge University Press.

Van Ark, E., & Lin, J. (2004). Time variations in igneous volume flux of the Hawaii-Emperor hot spot seamount chain. *Journal of Geophysical Research , 109*, B11401 .

Vidal, V., & Bonneville, A. (2004). Variations of the Hawaiian hot spot activity revealed by variations in the magma production rate. *Journal of Geophysical Research , 109*, B03104.

Wessel, P. (1998). An Empirical Method for Optimal Robust Regional-Residual Separation of Geophysical Data. *Mathematical Geology , 30* (4), 391-408.

Wessel, P. (1993). Observational Constraints on Models of the Hawaiian Hot Spot Swell. *Journal of Geophysical Research , 98* (B9), 16095-16104.

Wilson, J. T. (1963). A Possible Origin of the Hawaiian Islands. *Canadian Journal of Physics , 41*, 863-870.

Zhong, S., & Watts, A. B. (2002). Constraints on the dynamics of mantle plumes from uplift of the Hawaiian Islands. *Earth and Planetary Science Letters , 203* (1), 105-116.

Zhong, S., Ritzowoller, M., Shapiro, N., Landuyt, W., Huang, J., & Wessel, P. (2007). Bathymetry of the Pacific plate and its implications for thermal evolution of lithosphere and mantle dymanics. *Journal of Geophysical Research , 112*, B06412 .